Graphene as Cellular Interface: Electromechanical Coupling with Cells

Ravindra Kempaiah, Alfred Chung, and Vivek Maheshwari*

The Nanotechnology Engineering Program, Department of Chemistry, University of Waterloo, 200 University Avenue West, Waterloo, Canada N2L 3G1

ABSTRACT Interfacing cells with nanomaterials such as graphene, nanowires, and carbon nanotubes is useful for the integration of cellular physiology with electrical read outs. Here we show the interfacing of graphene sheets on the surface of yeast cells, leading to electromechanical coupling between the sheets and the cells. The cells are viable after the interfacing. The response caused by physiologically stressing the cells by exposure to alcohols, which causes a change in cell volume, can be observed in the electrical signal through graphene. The change in the cell volume leads to straining of the sheets, forming wrinkles which reduce the electrical conductivity. As the dynamic response of the cell can be observed, it is possible to differentiate between ethanol, 2-propanol, and water. We believe this will lead to further development of cell-based electrical devices and sensors.

KEYWORDS: cell · nano-bioelectronics · electromechanical coupling · dynamic cell response · graphene

Nanomaterials are being actively researched for making electrical interfaces with cells.[1−3] They have been used for sensing cellular responses with potential applications as sensors, biomedical devices, and energy harvesting systems.[4−9] In particular field effect transistors (FET) of nanowires, carbon nanotubes, and recently graphene have been used for this purpose.[2,3,10] The cells in these devices are placed over an FET forming a cellular−electrical interface. Here we show the interfacing of chemically reduced graphene (GR) sheets with eukaryotic yeast cells. The GR sheets deposit on the cell surface forming an electrically conductive layer and demonstrate electromechanical coupling to the cell. Since the GR sheets are on the cell surface, changes to cell volume and surface stresses can be observed. Such mechanical coupling can be used to study the dynamics of cell surface stresses, which are of importance in processes such as cell growth, division, and response to physiological factors such as osmotic stresses. In particular, GR sheets as two-dimensional electronic material have extremely high charge carrier mobility, high mechanical modulus and strength, and optical transparency.[11−14] The micrometer scale size makes GR sheets ideally suited for interfacing with surfaces of the cells without being transported into the cytoplasm. Their nanometer scale thickness and mechanical characteristics, makes the electrical conductivity of GR sheets highly sensitive to structural deformation (due to formation of ripples and folds).[15,16] This effect is used to electrically detect in real time the response of the cells to physiological stress upon exposure to ethanol and 2-propanol. As the transient change in conductivity can be recorded, the cells differential response to the applied stresses is characterized.

RESULTS AND DISCUSSION

Yeast cell, *Saccharomyces cerevisiae*'s (SaC) has been well characterized and is used extensively for development of new tools in biotechnology.[17] This makes it an ideal organism for development of bioelectrical devices to study cellular response. Here, its propensity to bind with Ca^{2+} ions is utilized for interfacing with GR sheets.[18] The basic scheme of the process is shown in Figure 1a (details in Supporting Information). Briefly, Ca^{2+} ions are bonded to citrate-functionalized gold nanoparticles (12 nm), forming Ca−Au.[19] Subsequently, graphene oxide (GO) sheets (prepared by Hummer's method)[20,21] due to their carboxylic and hydroxyl groups easily interface with the Ca−Au nanoparticles. The results of this binding are presented in field emission electron microscopy (FESEM) and transmission electron microscopy (TEM) images of Figure 1b,c, where Ca−Au nanoparticles with necklace-like morphology are seen attached on GO sheets. The GO−Ca−Au assembly is then reduced to GR−Ca−Au by using glucose and ammonium hydroxide.[22] The Raman spectra of graphene and graphene oxide show the characteristic G and D bands with the relative decrease in the intensity of the G band on reduction (Supporting Information).[23] The pH is kept neutral. For FESEM characterization the GR−Ca−Au sheets are absorbed on silica

* Address correspondence to vmaheshw@uwaterloo.ca.

Received for review May 16, 2011 and accepted June 15, 2011.

Published online June 15, 2011
10.1021/nn201791k

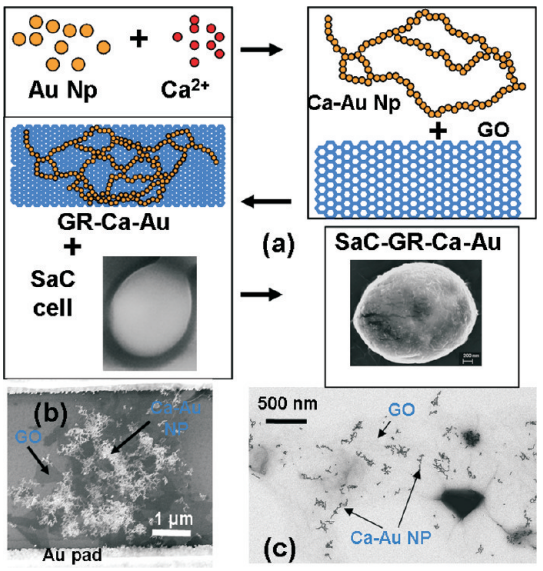

Figure 1. Graphene sheets are interfaced with yeast cells, SaC using calcium ion functionalized Au nanoparticles. (a) Au nanoparticles are functionalized with calcium ions transforming them into branched-chain assemblies. Subsequently, the Ca−Au nanoparticles are deposited on the GO sheets forming GO−Ca−Au assemblies that are reduced to form GR−Ca−Au. Yeast cells, SaC, are then interfaced with the GR−Ca−Au sheets using the calcium ion functionalization. (b) FESEM image showing GO sheets interface with the Ca−Au NP. The GO−Ca−Au assembly spans the ~4 μm gap across the Au pads on the Si chip. (c) TEM image shows qualitatively similar interfacing between the GO sheets and the Ca−Au NP.

substrates (plain substrate and also with patterned Au electrodes) after silane treatment (details in Supporting Information), hence there are no solvent evaporation effects. The TEM and FESEM images are qualitatively similar. The Ca^{2+} ions on the surface serve as the interface for binding of the GR sheets with yeast cells.

Yeast cells harvested at their initial log growth phase after washing twice are added to GR−Ca−Au solution (details in Supporting Information). After 1 h of incubation at room temperature the GR−Ca−Au cells are then deposited on silane-treated silica substrate with Au electrodes. FESEM analysis of the samples clearly shows the GR sheets on the surface of the cells with the Ca−Au nanoparticles (Figure 2a). Without the Ca−Au nanoparticles no significant deposition of the sheets on the cells is observed (Figure 2d), as both have a negative zeta potential in solution. The image also shows good contact between the electrodes and the GR sheets on the cells (Figure 2b). As the GR−Ca−Au sheets are deposited on the cell wall (which encapsulates the plasma membrane), it still permits a free functioning of the plasma membrane. Further the gaps between the deposited GR sheets (Figure 2a,c) allow the cells to sustain exchange processes with their surroundings, crucial to their survival. The results from a live−dead viability probe show that the cells maintain their metabolic activity and are healthy after interfacing with the GR−Ca−Au sheets (Figure 2e). For the viability test, GR−Ca−Au cells are incubated with FUN1 viability indicator and Calcofluor White. Metabolically viable cells uptake the FUN1 dye into vacuoles and shift its fluorescence to red from green (Figure 2e), hence, appearing as red spots in the cell. Calcofluor White has a blue fluorescence and stains only the cells wall, Figure. 2e.[24] Figure 2f is a stacked 3-D confocal image of the cell showing that the red spots from FUN1 are inside the cell and the blue fluorescence is on the surface (greater blue light intensity from the edge of cell) (more images in Supporting Information). The staining of the cell wall as blue and the presence of red fluorescence inside the cells also confirms that the dyes are able to diffuse through the gaps in the GR sheets and interact with the cell. Incubation of GR−Ca−Au sheets with FUN1 dye only leads to a decrease in the fluorescence intensity without any shift in the emission spectrum (Supporting Information).

To make an electronic cell, the GR−Ca−Au cells are deposited between gold electrodes patterned on silica substrate with spacing of ~2 μm. The current voltage characteristics of the cell are shown in Figure 3a. A linear response with no hysteresis is observed, indicating a good adhesion to the electrodes. Also Ca−Au cells deposited across the electrodes do not show any measurable current (Figure 3a), as the cell wall is primarily composed of carbohydrates and the Ca−Au nanoparticle chains deposited on the cells are in limited density and hence do not form a percolating pathway for electron conduction. The density is limited by the relative concentration of the Ca−Au nanoparticles to the cells. Similarly plain SaC cells also do not show any conduction (magnified images in Supporting Information). However GR−Ca−Au sheets form percolating pathways on interfacing with the SaC cells due to their sheet structure (2-D) that has a much larger surface area. The coupling of cellular response to GR sheets is observed when the cells are physiologically stressed by exposure to alcohol. As observed in Figure 3b, the conductance of the GR−Ca−Au cells decreases (reversibly) on briefly exposing them to ethanol (99%). The exposure time is limited (less than 3 min) to prevent permanent damage to the cells. Yeast cells show a decrease in cell volume and increase in surface roughness on exposure to alcohols (such as ethanol and 2-propanol).[25,26] This cellular response leads to compressive stresses on the GR sheets deposited on the cell surface. The stresses induce folds and ripples in GR sheets, increasing the scattering of charge carriers and thereby reducing the conductance of GR sheets, as observed. The decrease in conductance of GR−Ca−Au cell on exposure to alcohol is a two-step process, first there is an immediate decrease in the magnitude of the conductance (C_{step}, %), subsequently a more gradual rate of decrease is observed

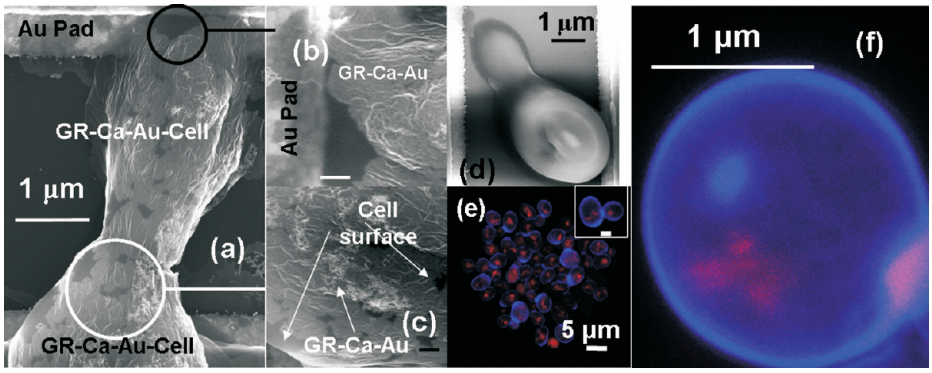

Figure 2. FESEM images showing the formation of the GR–Ca–Au cell (a) Two SaC cells spanning the gap between Au electrodes show clear deposition of the GR–Ca–Au sheets on their surface. The sheets deposit in high density on the cell with gaps in between exposing the cell surface. (b) An magnified view of the GR–Ca–Au cell on the Au pad shows good contact with GR sheets. (c) A magnified view of the cell surface shows the GR–Ca–Au sheets and the intermittently exposed cell surface. (d) Bare GR sheets without any Ca^{2+} ions fail to interface with the SaC cells. (e) Fluorescence analysis of the GR–Ca–Au cells with confocal microscopy. The yeast cells remain metabolically active after deposition of the GR–Ca–Au sheets as confirmed by the red fluorescence from FUN1 indicator. Calcofluor indicator stains the cell wall leading to a blue fluorescent cell outline. (f) 3-D fluorescence image from stacked confocal imaging shows that the blue fluoresce is on the surface and the red FUN1 staining is inside the cell.

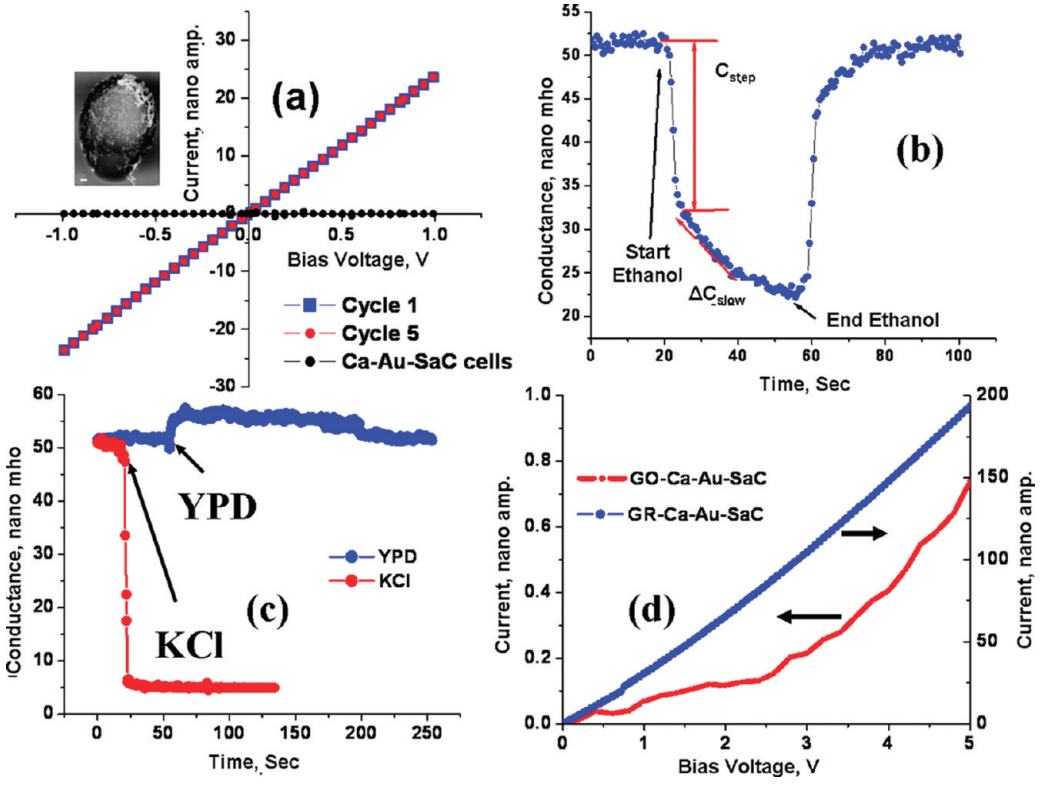

Figure 3. Current voltage characteristics of the cell device. (a) The electrical cell shows linear *I*–*V* characteristics over multiple cycles (first and fifth shown here), implying good contact with the electrodes. Ca–Au cells show no observable current on application of a bias voltage. Inset shows the FESEM image of a Ca–Au cell, and the scale bar is 150 nm. (b) When the cell is exposed to ethanol (99%) for 40 s., at 100 mV, a reversible drop in conductance is observed. (c) Similar to ethanol, exposure to 1 M KCl also leads to an instantaneous drop in conductance, while exposure to nutrient broth YPD shows an almost unchanged response with only a slight increase in conductance (<10%). (d) The conductance of SaC cells with Ca–Au–GO sheets is more than 2 orders of magnitude lower than cells with Ca–Au–GR sheets.

(ΔC_{slow}, mho/sec) (Figure 3b). To contrast this, plain GR–Ca–Au sheets on exposure to ethanol (and other alcohols) do not show any decrease in the current (Supporting Information). This signifies that the observed effect is not due to interaction between the alcohol and the graphene sheets. Further GO–Ca–Au–SaC cells show more than 2 orders of lower conductance than GR–Ca–Au cells, hence limiting their use for sensing of cellular response to physiological stresses (Figure 3d).[14] GR–Ca–Au cell on

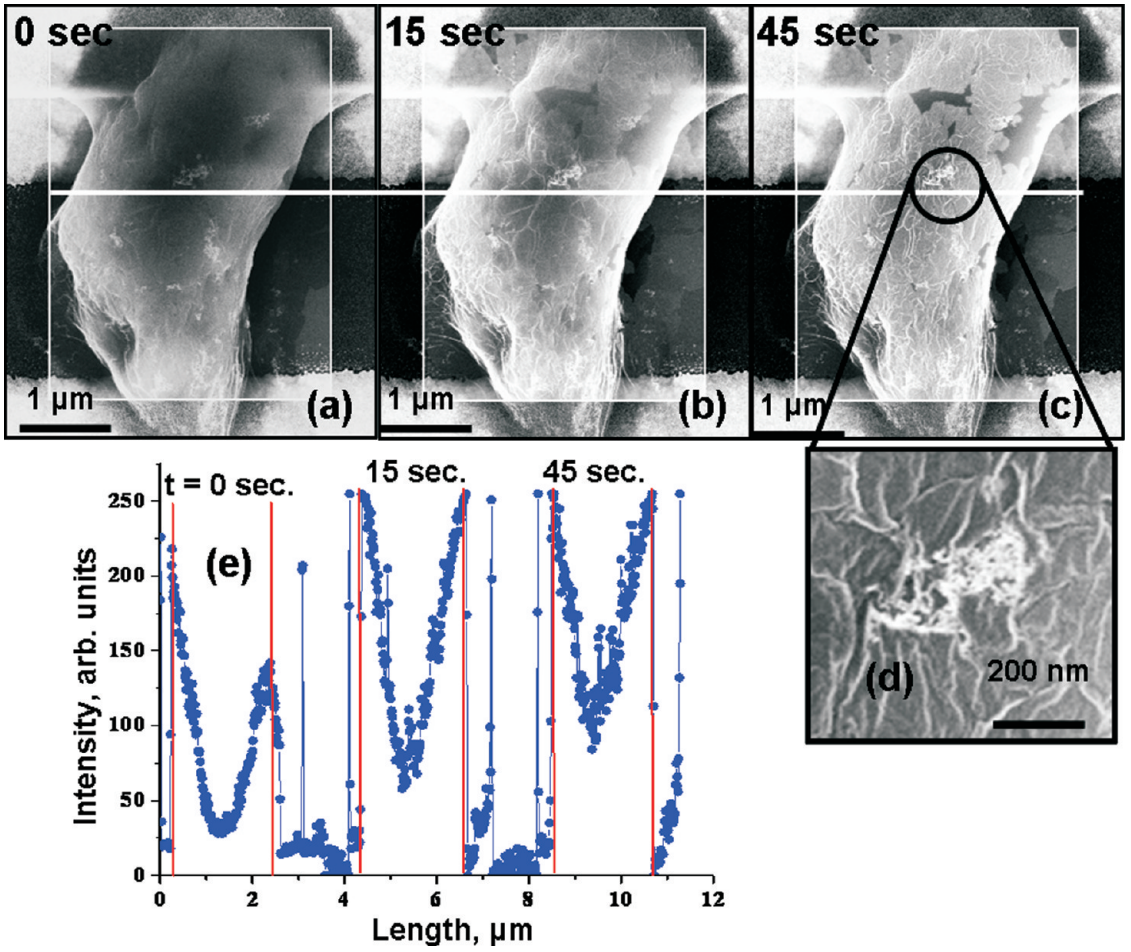

Figure 4. Exposure to electron beam in FESEM, similar to a heat shock, leads to a decrease in cell volume wrinkling the GR sheets on the yeast cells. Snapshots of the GR−Ca−Au cell at progressive exposure times, 0 (a), 15 (b), and 45 s (c), clearly show the effect. (d) A magnified view of the cell surface shows the wrinkles in the GR sheet. (e) The intensity plot of the line in panels a, b, and c shows that the lateral cell dimension decreases due to e-beam exposure.

exposure to 1 M KCl solution (due to hyperosmotic stress) also show a decrease in conductance, while in contrast on exposure to YPD nutrient broth the conductance is nearly constant with a very slight increase (Figure 3c). This shows the device response is due to the cell behavior rather than to the dielectric effects of the liquid or contact resistance, as each of these would be identical for 1 M KCl and YPD, both being in aqueous medium.

The stress shock to the cell due to exposure to alcohol is qualitatively similar to a heat shock in reducing the volume of the cell, leading to compressive stress.[26] Figure 4 panels a−c are a snapshot of GR−Ca−Au cell exposed continuously to a FESEM e-beam (a heat shock). The cell volume shrinks with exposure, and the GR sheets on the surface start to wrinkle. The cell shrinkage as calculated from the line scan shown in Figure 4e leads to lateral strains of 4.4% and 7.8% after 15 and 45 s exposure. This lays the basis for the observed decrease in the current on exposing the GR−Ca−Au cells to alcohol. Also optical images of SaC cells before and after exposure to 70% ethanol for 10 min show the decrease in cells volume (Supporting Information). Prolonged exposure to alcohol for more than 10 min leads to permanent decrease in the current, signifying lasting damage to the cell. The roughness of a GR−Ca−Au cell exposed to ethanol (10 min) is directly observed in atomic force microscopy (AFM) images (Figure 5a−c); clearly visible are the surface wrinkles on the cell confirming the deformation of the GR sheets due to the stress shock. The deformations are 10−25 nm in height and appear at a regular interval (Figure 5c). Unexposed cells have a smooth surface with surface roughness of less than 2 nm.[27]

The dynamic response of the cell (decrease in cell volume and increase in surface roughness) to alcohol is governed by the hydrophobic nature of the alcohol, which affects its ability to penetrate through the plasma membrane.[28] A more hydrophilic component aiding the alcohol's rapid penetration into the cell leads to a faster response. Since the cell is coupled to GR sheets, the rate of the cellular response is reflected in the conductivity of the GR−Ca−Au cell device.

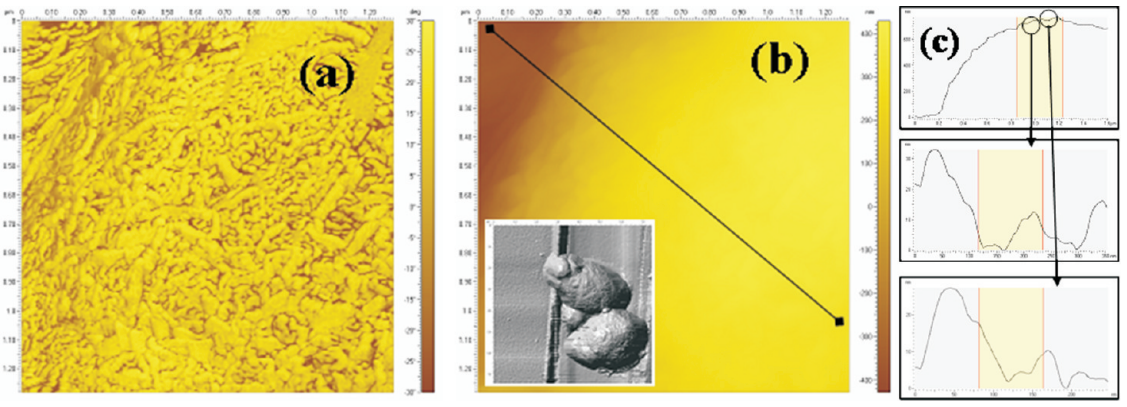

Figure 5. AFM images of GR−Ca−Au cells after exposure to ethanol showing the cell surface roughness and formation of undulations that strain the GR sheets: (a) phase image, (b) height image of the surface of a cell deposited between Au electrodes on a silicon dioxide chip (inset of b). The images are 1.3 μm square. (c) The profile of the cell surface along the line marked in panel b shows a cell height of ~0.75 μm. The vertical scale is up to 760 nm and the horizontal is up to 1.6 μm. The magnified profile along the line shows the undulations on the surface are 10−25 nm in height. The vertical scale is 33 and 27 nm and the horizontal scale is 350 and 290 nm, respectively, in the magnified views.

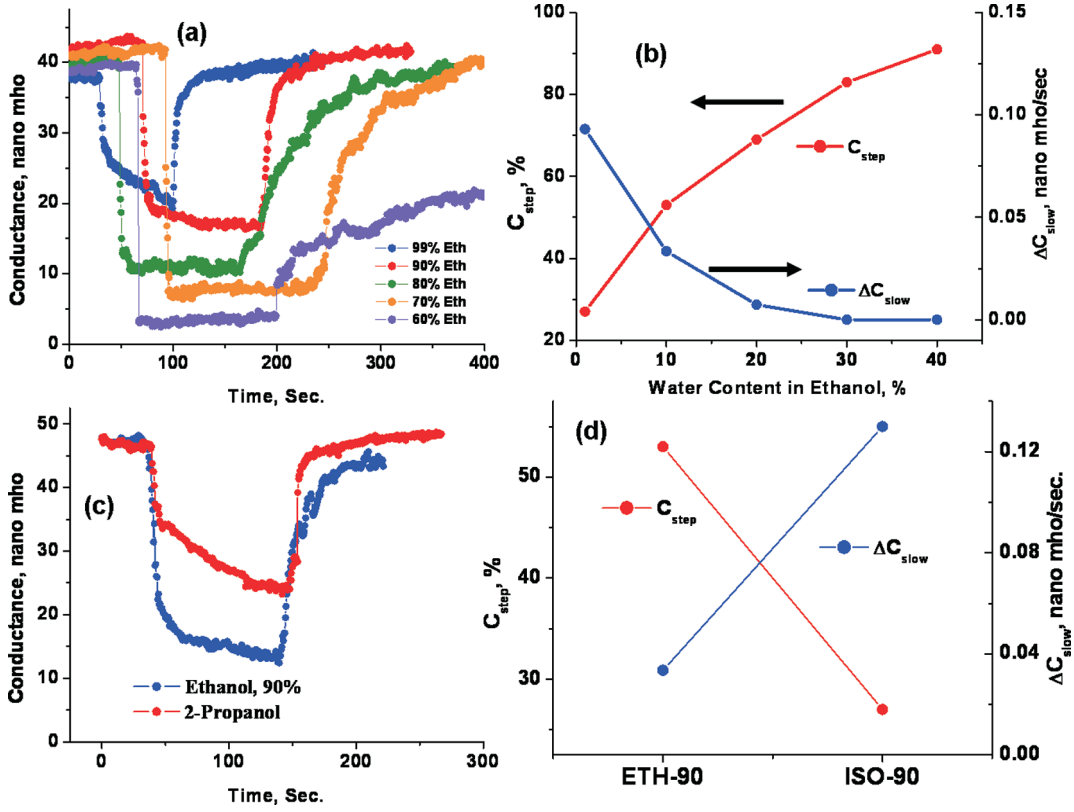

Figure 6. Exposure of the GR−Ca−Au cell to ethanol and 2-propanol solutions at 100 mV produces a dynamic response from the cell which is observed as change in conductance of the GR layer. (a) Increasing water content in the alcohol solution results in a faster response from the cell, leading to a rapid change in conductance. (b) The parameters C_{step} and ΔC_{slow} quantify the response from the cell. Increasing water content leads to a larger C_{step}, while reducing the ΔC_{slow}. (c) A similar trend is observed on exposing the cell to 90% 2-propanol. In comparison to 90% ethanol, the cell response is slower as quantified in panel d.

The two observed parameters C_{step} and ΔC_{slow} are used to characterize the response of the cell to the alcohol stress shock. To this effect, the GR−Ca−Au cell is exposed to five different concentrations of ethanol (99%, 90%, 80%, 70%, and 60% by volume), Figure 6a. As observed the initial step decrease in conductivity, C_{step}, becomes larger in magnitude with increasing water content (individual figures in Supporting Information). Figure 6b summarizes the results from the stress shocks to the GR−Ca−Au cells. Further irreversible change in conductivity is observed when the GR−Ca−Au cell is exposed to 60% ethanol

solution, implying a permanent change to the cell morphology. This signifies that 60% v/v fraction of ethanol is most effective in penetrating the cell. Similarly using 2-propanol (90%) reduces the initial step decrease in conductivity, C_{step} (Figure 6c,d). The gradual decrease, ΔC_{slow}, of the conductivity becomes significant with the increasing hydrophobic nature of the solution. The dual nature of the response (a fast one, C_{step} and a more gradual one, ΔC_{slow}) can arise from an initial rapid change of the cell morphology due to penetration of the alcohol. The slower response (ΔC_{slow}) arises for alcohol solutions that are slow to permeate into the cell due to their greater hydrophobic component and hence generate a lagged response. Since these measurements are made on the same cell the surface coverage of GR is identical for all results. Qualitatively identical results were observed with other GR−Ca−Au cells, irrespective of the order of measurement (except 60% ethanol solution was always the last exposure). The permanent change to cell morphology with 60% ethanol solution matches well with its common use as an antiseptic agent.

CONCLUSION

The formation of the GR−Ca−Au cell demonstrates the interfacing of GR sheets with live cells. The sheets form an electron conducting pathway on the surface of the cell. The interfacing with the cell is accomplished by the use of calcium ions coated Au nanoparticles as the biocompatible moiety. As the GR sheets are nanometer in thickness with their reported modulus in the range of 1 TPa,[12] they deform easily to compressive stresses leading to formation of folds and wrinkles. A 15% percent decrease in cell volume (due to 5% strain in lateral dimensions, Figure 4e) will lead to stresses on the order of 22.5 MPa (bulk modulus of cell wall is taken as 150 MPa).[29] This stress will easily wrinkle the GR sheets. The height of the wrinkles is ∼14 nm as calculated to these stresses by taking the sheets as 500 nm squares (FESEM images in Supporting Information) with a thickness of 1.5 nm (AFM images of GR sheets in Supporting Information).[16] This matches with the observed size of deformations on the cell surfaces by AFM ≈ 10−25 nm (Figure 5c). The reduction in conductivity due to formation of wrinkles is used to observe in real time the effect of stress shock (exposure to alcohol) on yeast cells. A two-step process is observed: an immediate reaction to the alcohol and a more subtle gradual response. Further it is observed that the cell responds with faster dynamics on increasing the hydrophilic nature of the alcohol solution.

Interfacing GR sheets with cells can be expanded to couple with other cellular responses such as cell growth and ion channel dynamics. The signal transduction by GR can result from changes in surface stresses or the chemical potential due to the flow of ions such as H^+. A detailed study of the effect of GR sheets on the cellular activity will further advance the field. Examples of the cell on FET-type devices have shown that cells maintain their biochemical and bioelectrical activity. Since GR sheets are impermeable membranes, for cells lacking the cell wall, the degree of deposition can be controlled by use of sheets with well-defined size and concentration (*e.g.*, refined by centrifugation).[30] This will limit the cell surface area covered by GR sheets while still maintaining the conductivity and cellular activity. The sensitivity of the device can be further improved by using pristine graphene instead of chemically reduced graphene. However this will need development of solution processing methods to deposit the pristine graphene on the cell surface. Chemically reduced graphene has been used for making electrochemical sensors[31,32] and the detection of surface doping by cells and polymers.[33] The advantage of using GO is also due to its colloidal stability and surface functionalization that can be used for attaching targeting molecules for interfacing with cells.[34] Cell proliferation is also modulated by mechanical stimulus; such observations can be coupled to an electrical sensor using the GR sheets. Similarly growth of cells (increase in the cell volume) and their division will also create stresses on the sheets leading to a change in the electrical signal. Compared to biochemical processes these transformations are long lasting and hence should result in a sustained change of the electrical signal. Further the large area of GR sheets can also be useful for harvesting of energy from cellular organism, development of cells as template to make GR devices and biomaterials.

METHODS

Graphene oxide was made by modified Hummers method (details in Supporting Information).[20,21] Following this Ca−Au[19] was prepared and mixed with GO solution (details in Supporting Information). The GO was then chemically reduced with glucose forming chemically reduced graphene (GR).[22] Yeast cell grown in YPD broth were washed and mixed with the GR−Ca−Au solution for interfacing. Subsequently the cells were imaged with FESEM, TEM by deposition on silane functionalized silicon chips (and chips with patterned Au electrodes). For testing the viability of cells, the GR−Ca−Au interfaced yeast cells were targeted with FUN1 and Calcofluor fluorescent reagents, from Molecular probes L-7009 LIVE/DEAD Yeast Viability Kit (Invitrogen) (details in Supporting Information). The current−voltage characteristics of the chemically reduced graphene interfaced cells were tested using a home-built setup and a simple flow cell (details in the Supporting Information).

Acknowledgment. This work was supported by the University of Waterloo start up funds, Canada Foundation for

Innovation (LOF 25431), and Ministry of Research and Innovation, Ontario. The authors also thank N. Heinig for help with AFM and FESEM analysis.

Supporting Information Available: Experimental details; characterization results from AFM, FESEM, TEM, optical microscopy, absorption spectroscopy, fluorescence spectroscopy, Raman spectroscopy, confocal microscopy, and current–voltage measurements. This material is available free of charge *via* the Internet at http://pubs.acs.org.

REFERENCES AND NOTES

1. Jan, E.; Hendricks, J. L.; Husaini, V.; Richardson-Burns, S. M.; Sereno, A.; Martin, D. C.; Kotov, N. A. Layered Carbon Nanotube–Polyelectrolyte Electrodes Outperform Traditional Neural Interface Materials. *Nano Lett.* **2009**, *9*, 4012–4018.
2. Cohen-Karni, T.; Qing, Q.; Li, Q.; Fang, Y.; Lieber, C. M. Graphene and Nanowire Transistors for Cellular Interfaces and Electrical Recording. *Nano Lett.* **2010**, *10*, 1098–1102.
3. Cohen-Karni, T.; Timko, B. P.; Weiss, L. E.; Lieber, C. M. Flexible Electrical Recording from Cells Using Nanowire Transistor Arrays. *Proc. Natl. Acad. Sci. U.S.A.* **2009**, *106*, 7309–7313.
4. Dhar, S.; Liu, Z.; Thomale, J.; Dai, H. J.; Lippard, S. J. Targeted Single-Wall Carbon Nanotube-Mediated Pt(IV) Prodrug Delivery Using Folate as a Homing Device. *J. Am. Chem. Soc.* **2008**, *130*, 11467–11476.
5. Kam, N. W. S.; Jan, E.; Kotov, N. A. Electrical Stimulation of Neural Stem Cells Mediated by Humanized Carbon Nanotube Composite Made with Extracellular Matrix Protein. *Nano Lett.* **2009**, *9*, 273–278.
6. Fang, Z. C.; Soleymani, L.; Pampalakis, G.; Yoshimoto, M.; Squire, J. A.; Sargent, E. H.; Kelley, S. O. Direct Profiling of Cancer Biomarkers in Tumor Tissue Using a Multiplexed Nanostructured Microelectrode Integrated Circuit. *ACS Nano* **2009**, *3*, 3207–3213.
7. Shalek, A. K.; Robinson, J. T.; Karp, E. S.; Lee, J. S.; Ahn, D. R.; Yoon, M. H.; Sutton, A.; Jorgolli, M.; Gertner, R. S.; Gujral, T. S.; *et al*. Vertical Silicon Nanowires as a Universal Platform for Delivering Biomolecules into Living Cells. *Proc. Natl. Acad. Sci. U.S.A.* **2010**, *107*, 1870–1875.
8. Qing, Q.; Pal, S. K.; Tian, B. Z.; Duan, X. Z.; Timko, B. P.; Cohen-Karni, T.; Murthy, V. N.; Lieber, C. M. Nanowire Transistor Arrays for Mapping Neural Circuits in Acute Brain Slices. *Proc. Natl. Acad. Sci. U.S.A.* **2010**, *107*, 1882–1887.
9. Ryu, W.; Bai, S. J.; Park, J. S.; Huang, Z. B.; Moseley, J.; Fabian, T.; Fasching, R. J.; Grossman, A. R.; Prinz, F. B. Direct Extraction of Photosynthetic Electrons from Single Algal Cells by Nanoprobing System. *Nano Lett.* **2010**, *10*, 1137–1143.
10. Lovat, V.; Pantarotto, D.; Lagostena, L.; Cacciari, B.; Grandolfo, M.; Righi, M.; Spalluto, G.; Prato, M.; Ballerini, L. Carbon Nanotube Substrates Boost Neuronal Electrical Signaling. *Nano Lett.* **2005**, *5*, 1107–1110.
11. Novoselov, K. S.; Geim, A. K.; Morozov, S. V.; Jiang, D.; Zhang, Y.; Dubonos, S. V.; Grigorieva, I. V.; Firsov, A. A. Electric Field Effect in Atomically Thin Carbon Films. *Science* **2004**, *306*, 666–669.
12. Lee, C.; Wei, X. D.; Kysar, J. W.; Hone, J. Measurement of the Elastic Properties and Intrinsic Strength of Monolayer Graphene. *Science* **2008**, *321*, 385–388.
13. Kim, K. S.; Zhao, Y.; Jang, H.; Lee, S. Y.; Kim, J. M.; Kim, K. S.; Ahn, J. H.; Kim, P.; Choi, J. Y.; Hong, B. H. Large-Scale Pattern Growth of Graphene Films for Stretchable Transparent Electrodes. *Nature* **2009**, *457*, 706–710.
14. Kaiser, A. B.; Gomez-Navarro, C.; Sundaram, R. S.; Burghard, M.; Kern, K. Electrical Conduction Mechanism in Chemically Derived Graphene Monolayers. *Nano Lett.* **2009**, *9*, 1787–1792.
15. de Parga, A. L. V.; Calleja, F.; Borca, B.; Passeggi, M. C. G.; Hinarejos, J. J.; Guinea, F.; Miranda, R. Periodically Rippled Graphene: Growth and Spatially Resolved Electronic Structure. *Phys. Rev. Lett.* **2008**, *100*, 056807.
16. Bao, W. Z.; Miao, F.; Chen, Z.; Zhang, H.; Jang, W. Y.; Dames, C.; Lau, C. N. Controlled Ripple Texturing of Suspended Graphene and Ultrathin Graphite Membranes. *Nat. Nanotechnol.* **2009**, *4*, 562–566.
17. Murray, D. B.; Beckmann, M.; Kitano, H. Regulation of Yeast Oscillatory Dynamics. *Proc. Natl. Acad. Sci. U.S.A.* **2007**, *104*, 2241–2246.
18. Maheshwari, V.; Fomenko, D. E.; Singh, G.; Saraf, R. F. Ion Mediated Monolayer Deposition of Gold Nanoparticles on Microorganisms: Discrimination by Age. *Langmuir* **2010**, *26*, 371–377.
19. Maheshwari, V.; Kane, J.; Saraf, R. F. Self-Assembly of a Micrometers-Long One-Dimensional Network of Cemented Au Nanoparticles. *Adv. Mater.* **2008**, *20*, 284–287.
20. Hummers, W. S.; Offeman, R. E. Preparation of Graphitic Oxide. *J. Am. Chem. Soc.* **1958**, *80*, 1339.
21. Kovtyukhova, N. I.; Ollivier, P. J.; Martin, B. R.; Mallouk, T. E.; Chizhik, S. A.; Buzaneva, E. V.; Gorchinskiy, A. D. Layer-by-layer Assembly of Ultrathin Composite Films from Micron-Sized Graphite Oxide Sheets and Polycations. *Chem. Mater.* **1999**, *11*, 771–778.
22. Zhu, C. Z.; Guo, S. J.; Fang, Y. X.; Dong, S. J. Reducing Sugar: New Functional Molecules for the Green Synthesis of Graphene Nanosheets. *ACS Nano* **2010**, *4*, 2429–2437.
23. Stankovich, S.; Dikin, D. A.; Piner, R. D.; Kohlhaas, K. A.; Kleinhammes, A.; Jia, Y.; Wu, Y.; Nguyen, S. T.; Ruoff, R. S. Synthesis of Graphene-Based Nanosheets *via* Chemical Reduction of Exfoliated Graphite Oxide. *Carbon* **2007**, *45*, 1558–1565.
24. Wang, B.; Liu, P.; Jiang, W. G.; Pan, H. H.; Xu, X. R.; Tang, R. K. Yeast Cells with an Artificial Mineral Shell: Protection and Modification of Living Cells by Biomimetic Mineralization. *Angew. Chem., Int. Ed.* **2008**, *47*, 3560–3564.
25. Canetta, E.; Adya, A. K.; Walker, G. M. Atomic Force Microscopic Study of the Effects of Ethanol on Yeast Cell Surface Morphology. *FEMS Microbiol. Lett.* **2006**, *255*, 308–315.
26. Piper, P. W. The Heat-Shock and Ethanol Stress Responses of Yeast Exhibit Extensive Similarity and Functional Overlap. *FEMS Microbiol. Lett.* **1995**, *134*, 121–127.
27. Ahimou, F. O.; Touhami, A.; Dufrene, Y. F. Real-Time Imaging of the Surface Topography of Living Yeast Cells by Atomic Force Microscopy. *Yeast* **2003**, *20*, 25–30.
28. Bemporad, D.; Essex, J. W.; Luttmann, C. Permeation of Small Molecules through a Lipid Bilayer: A Computer Simulation Study. *J. Phys. Chem. B* **2004**, *108*, 4875–4884.
29. Hartmann, C.; Delgado, A. Numerical Simulation of the Mechanics of a Yeast Cell under High Hydrostatic Pressure. *J. Biomech.* **2004**, *37*, 977–987.
30. Sun, X.; Luo, D.; Liu, J.; Evans, D. G. Monodisperse Chemically Modified Graphene Obtained by Density Gradient Ultracentrifugal Rate Separation. *ACS Nano* **2010**, *4*, 3381–3389.
31. Zhou, M.; Zhai, Y. Electrochemical Sensing and Biosensing Platform Based on Chemically Reduced Graphene Oxide. *Anal. Chem.* **2009**, *81*, 5603–5613.
32. Wang, Z.; Zhou, X.; Zhang, J.; Boey, F.; Zhang, H. Direct Electrochemical Reduction of Single-Layer Graphene Oxide and Subsequent Functionalization with Glucose Oxidase. *J. Phys. Chem. C.* **2009**, *113*, 14071–14075.
33. Mohanty, N.; Berry, V. Graphene-Based Single-Bacterium Resolution Biodevice and DNA Transistor: Interfacing Graphene Derivatives with Nanoscale and Microscale Biocomponents. *Nano Lett.* **2008**, *8*, 4469–4476.
34. Liu, Z.; Robinson, J. T.; Sun, X.; Dai, H. PEGylated Nanographene Oxide for Delivery of Water-Insoluble Cancer Drugs. *J. Am. Chem. Soc.* **2008**, *130*, 10876–10877.